Supplement of Atmos. Chem. Phys., 19, 15073–15086, 2019
https://doi.org/10.5194/acp-19-15073-2019-supplement

Atmospheric Chemistry and Physics
Open Access
EGU

Supplement of

Effect of NO_x on 1,3,5-trimethylbenzene (TMB) oxidation product distribution and particle formation

Epameinondas Tsiligiannis et al.

Correspondence to: Mattias Hallquist (hallq@chem.gu.se)

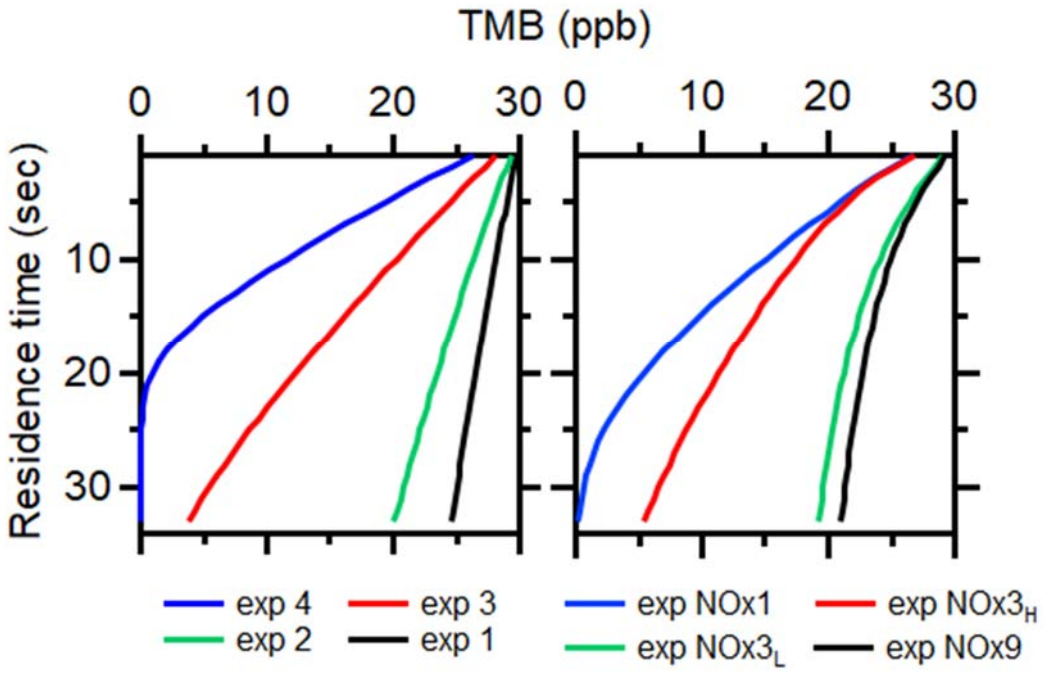

Figure S1: Vertical profile of TMB (ppb) in the PAM chamber without (left) and with NO_x (right).

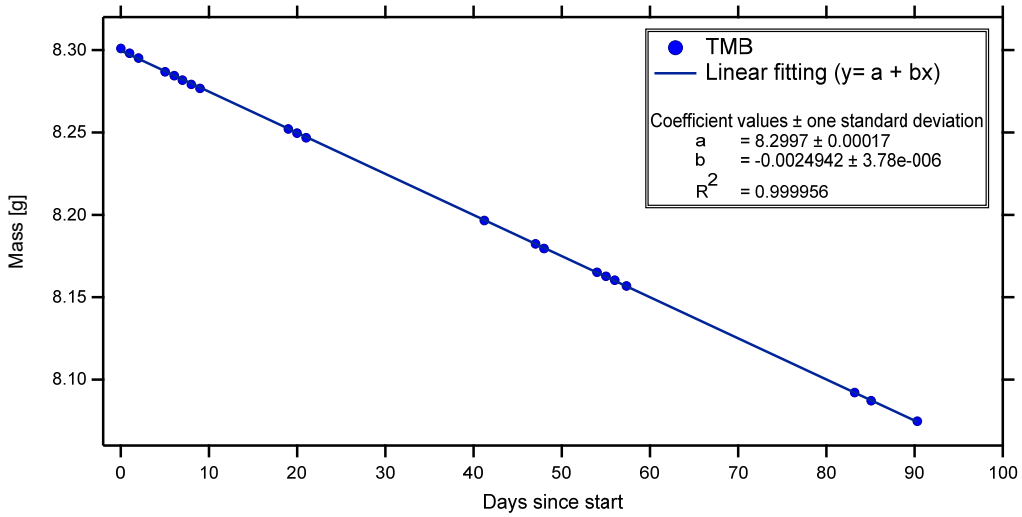

Figure S2: Characterization of TMB evaporation rate from the diffusion vial at a temperature of 20°C.

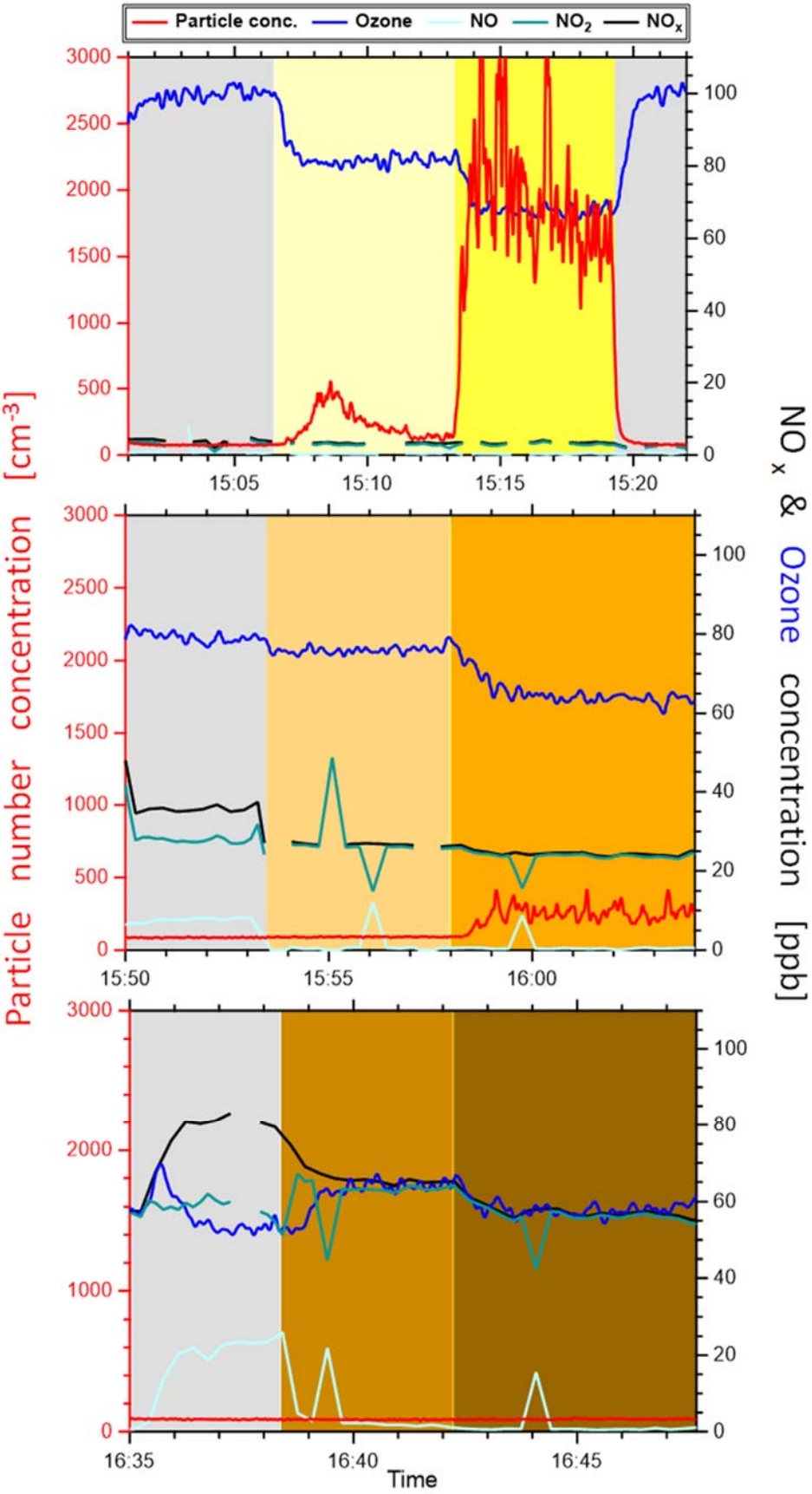

Figure S3: Particle number (red), ozone (blue), NO_x (black), NO (light blue) and NO_2 (cyan) concentrations under NO_x free conditions (top panel), initial NO_x:VOC≈1 (middle panel) and NO_x:VOC≈3 (bottom panel). The grey areas represent dark conditions, the light yellow, orange and brown represent lower OH exposure conditions (using one UV lamp) and the dark yellow, orange and brown represent higher OH exposure conditions (using two UV lamps).

Table S1: Contribution of the highest 10 compounds depending on experimental condition.

1		**2**		**3**		**4**	
$C_9H_{12}O_{10}$	4.44	$C_{18}H_{26}O_{10}$	4.76	$C_{18}H_{26}O_{10}$	5.68	$C_9H_{14}O_7$	5.48
$C_{18}H_{26}O_{10}$	4.04	$C_{18}H_{28}O_{11}$	4.53	$C_{18}H_{28}O_{11}$	4.86	$C_9H_{16}O_9$	4.64
$C_{18}H_{28}O_{11}$	3.46	$C_9H_{15}O_8$	3.83	$C_{18}H_{28}O_{12}$	4.55	$C_9H_{14}O_8$	4.49
$C_9H_{15}NO_{10}$	3.07	$C_9H_{14}O_7$	3.19	$C_9H_{14}O_7$	4.27	$C_9H_{16}O_8$	4.48
$C_9H_{13}NO_8$	2.87	$C_9H_{14}O_8$	3.04	$C_9H_{16}O_8$	4.02	$C_{18}H_{28}O_{12}$	3.60
$C_9H_{15}O_8$	2.87	$C_9H_{15}NO_{10}$	2.93	$C_9H_{16}O_9$	3.70	$C_9H_{14}O_6$	3.10
$C_9H_{14}O_8$	2.82	$C_9H_{12}O_{10}$	2.62	$C_9H_{14}O_8$	3.31	$C_9H_{14}O_9$	2.91
$C_9H_{12}O_9$	2.30	$C_9H_{16}O_8$	2.42	$C_9H_{15}O_8$	2.94	$C_9H_{16}O_7$	2.85
$C_{18}H_{25}O_{13}$	2.13	$C_9H_{15}O_7$	2.20	$C_9H_{16}O_7$	2.69	$C_{18}H_{26}O_{10}$	2.84
$C_9H_{15}NO_8$	2.11	$C_9H_{16}O_9$	2.18	$C_{18}H_{26}O_{12}$	2.64	$C_{18}H_{26}O_{12}$	2.68
total	28.6		29.8		38.7		35.9
$NOx3_L$		**NOx9**		**NOx1**		**$NOx3_H$**	
$C_9H_{14}N_2O_{10}$	10.0	$C_9H_{14}N_2O_{10}$	16.0	$C_9H_{15}NO_{10}$	6.1	$C_9H_{15}NO_{10}$	10.4
$C_9H_{13}NO_7$	7.0	$C_9H_{13}NO_7$	15.6	$C_9H_{14}O_7$	3.7	$C_9H_{14}N_2O_{10}$	5.8
$C_9H_{15}NO_8$	6.6	$C_9H_{13}NO_8$	6.1	$C_9H_{16}O_9$	3.4	$C_9H_{13}NO_8$	3.9
$C_9H_{13}NO_8$	5.2	$C_9H_{12}O_{10}$	3.1	$C_9H_{14}O_8$	3.4	$C_9H_{15}NO_8$	2.4
$C_9H_{12}O_{10}$	4.0	$C_9H_{13}NO_9$	2.4	$C_9H_{16}O_8$	3.0	$C_9H_{14}O_7$	2.2
$C_9H_{14}O_8$	2.1	$C_9H_{15}NO_{10}$	2.3	$C_9H_{14}O_6$	2.5	$C_9H_{14}O_8$	2.1
$C_9H_{15}NO_8$	2.1	$C_9H_{12}O_9$	1.9	$C_9H_{14}O_9$	2.3	$C_9H_{13}NO_9$	2.0
$C_9H_{13}NO_9$	2.0	$C_9H_{14}O_8$	1.8	$C_{18}H_{28}O_{12}$	2.1	$C_9H_{14}O_6$	2.0
$C_9H_{12}O_9$	1.8	$C_9H_{14}N_2O_9$	1.7	$C_9H_{15}O_8$	2.0	$C_9H_{12}O_{10}$	1.8
$C_9H_{13}NO_8$	1.7	$C_9H_{13}NO_{10}$	1.6	$C_{18}H_{26}O_{10}$	1.9	$C_9H_{13}NO_7$	1.6
total	42.3		52.4		30.5		34.2

Kinetic model of HOM and ON formation in PAM chamber

A chemical model, describing comprehensively the ozone photolysis at 254nm and NO_x chemistry as well as the general scheme for HOM formation by 1,3,5 trimethylbenzene (TMB) in the Go:PAM, was used. The main structure of the model is based on Watne et al. (2018), where the rate coefficients are adapted from Sander et al. (2011) and Li et al. (2015). The new NO_x chemistry are based on Atkinson et al. (1992); Finlayson-Pitts (1999) and Berndt et al. (2018), while the regular TMB oxidation scheme was taken from the MCM v3.3.1 (Jenkin et al., 2003) and the more oxidized one from Ehn et al. (2014); Wang et al. (2017); Jenkin et al. (2019); Berndt et al. (2018) and Zhao et al. (2018). All the reaction and the corresponding rate constants are given in Table S2. FACSIMILE 4 (FACSIMILE for Windows 4, 2009) was used to implement the model and solve the differential equations.

The photon flux at 254nm used in the simulations was tuned to match measured decay of O_3 and was calculated to be $P_{FLUX254} = 1.31\times10^{16}$ $cm^{-2}s^{-1}$. A OH sink was added to match the observed OH production in the background experiment, i.e. without the addition of TMB. The model was run for all experiments with and without NO_x. HOM (MONOMER) were produced as a termination product from $HOMRO_2$ or the corresponding alkoxy radical (HOMRO). According to the oxygen content in the majority of the C_9 products the oxidized peroxy radicals ($HOMRO_2$) should contain either seven, nine or eleven oxygen which would be formed after two, three or four autoxidation steps, respectively. To simplify the model the produced $HOMRO_2$ in the model were assumed to be formed after 3 autoxidation steps. There are large uncertainties on estimating the rate coefficients for the autoxidation step (Jenkin et al., 2019). The following assumptions were taken in account for our best lumped estimation of the three step oxidation. The 1st step where the O_2 group make a bicyclic radical most likely has a large rate coefficient where Jenkin et al., 2019 suggests a rate coefficient for similar reactions to be larger than 3.6×10^2 s^{-1} (Jenkin et al., 2019). For the 2nd step we assume an internal hydrogen shift potentially facilitated by a conjugated three carbon system. Here Wang et al., 2017 give a large range in reaction rates for similar reactions where the radical from toluene is slow (2.6×10^{-2} s^{-1}) while the radical from larger compounds has higher values (e.g. 7.0 s^{-1}). We use a value of 1 s^{-1} to represent this 2nd step. For the 3rd step that would represent another hydrogen shift we use the value of 0.5 s^{-1} originally suggested in the paper by Ehn et al., 2014. The combined rate of these three subsequent steps would then be 0.33 s^{-1}. The oxidation state of produced dimers was defined as low, medium or high, depending on the cross reactions. A cross reaction between a general RO_2 and another RO_2 leads to low oxidized dimer (LODIMER), between a RO_2 and $HOMRO_2$ leads to medium oxidized dimer (MODIMER) and between a $HOMRO_2$ and another $HOMRO_2$ leads to high oxidized dimer (HODIMER). Highly oxygenated nitrates (ON) was formed via $HOMRO_2$ reaction with NO.

Three different cases were tested, in which the rate coefficients of the cross reactions (Reactions 63 – 68) were varied. During the 1st case the rate coefficients of the following reactions (Reactions 63, 64, 66 and 67) was 8.8×10^{-13} cm3 $molecules^{-1}$ s^{-1} (MCM) and the dimer formation reactions (Reactions 65 and 68) were based on Berndt et al. (2018). In that case either we overestimate the production of dimers, underestimate the production of monomers or both of them. The concentration of dimers dominates even in the experiments with high NO_x, which is not consistent with our measurements. In the 2nd case the rate coefficient of Reactions 65 and 68 were kept constant, but for the rest of them changed to 1×10^{-12} cm^3 $molecules^{-1}$ s^{-1} based on Zhao et al. (2018). The concentration of the dimers was still quite higher than the monomers and nitrates, even in the high NO_x experiments. This overestimation suggests that the rate coefficients of the reactions, in which dimers are produced, are lower. Thus, during the 3rd case the rate coefficients for the reactions 65 and 68 were decreased to 2×10^{-12} cm^3 $molecules^{-1}$ s^{-1} (Zhao et al., 2018). The same value was used for both dimer formation reactions, in contrast to the 1st and 2nd cases. The 3rd case gives the best results compared to our measurements (see main text).

Table S2: Reactions and rate coefficients for model calculations. Rate constants were taken from Sander et al. (2011), Li et al. (2015). and Jenkin et al., (2003) unless otherwise stated. The temperature was 298 K, the relative humidity was 38% and the pressure (M = 2.46×10^{19} molecules cm^{-3}).

No.	*Reaction*	*k*	*Comments*
1	O3 + hν → O2 + O(1D)	0.15	$\sigma_{254}=1.148\times10^{-17}cm^{-2}$
2	O(1D) + H2O → OH + OH	1.99×10^{-10}	
3	O(1D) + O2 → O(3P) + O2	3.97×10^{-11}	
4	O(1D) + O3 → O2 + O(3P) + O(3P)	1.2×10^{-10}	
5	O(1D) + O3 → O2 + O2	1.2×10^{-10}	
6	O(1D) + N2 → O(3P) + N2	3.11×10^{-11}	
7	O(3P) + O2 + M → O3 +M	6.1×10^{-34}	
8	O(3P) + O3 → O2 + O2	7.96×10^{-15}	
9	O(3P) + OH → H + O2	3.29×10^{-11}	
10	H + O2 → HO2	9.57×10^{-13}	
11	H + HO2 → OH + OH	7.2×10^{-11}	
12	H + HO2 → O(3P) + H2O	1.6×10^{-12}	
13	H + HO2 → H2 + O2	6.9×10^{-12}	
14	OH + OH → H2O + O(3P)	1.8×10^{-12}	
15	OH + OH → H2O2	6.29×10^{-12}	
16	OH + O3 → HO2 + O2	7.25×10^{-14}	
17	HO2 + HO2 → H2O2 + O2	3.28×10^{-12}	$(k_{17} = 3\times10^{-13}\times e^{(460/T)}+2.1\times10^{-33}\times e^{(920/T)}\times M) \times (1+1.4\times10^{-21}) \times H_2O\times e^{(2200/T)}$
18	OH + TMB → 0.82 RO2	5.67×10^{-11}	MCM
19	OH + TMB → 0.18 HO2	5.67×10^{-11}	MCM
20	NO + O(3P) → NO2	1.66×10^{-12}	
21	O(3P) + OH → H + O2	3.29×10^{-11}	
22	NO2+ hν → NO + O(3P)	1.37×10^{-4}	$\sigma_{254}=1.05\times10^{-20}$
23	OH + NO2 → HNO3	1.06×10^{-11}	
24	OH + NO2 → HOONO	1.79×10^{-12}	
25	HO2 + NO → OH + NO2	8.16×10^{-12}	
26	RO2 + NO → RO + NO2	9.0×10^{-12}	MCM
27	O(1D) + N2 + M → N2O + M	2.82×10^{-36}	
28	N2O + O(1D) → N2 + O2	5.09×10^{-11}	
29	N2O + O(1D) → NO + NO	7.64×10^{-11}	
30	O(3P) + HO2 → OH + O2	5.87×10^{-11}	
31	O(3P) + H2O2 → OH + HO2	1.7×10^{-15}	
32	H + O3 → OH + O2	2.89×10^{-11}	
33	HO2 + O3 → OH + O2 +O2	1.93×10^{-15}	
34	HO2 + OH → H2O + O2	1.11×10^{-10}	
35	H2O2 + hν → OH +OH	8.75×10^{-4}	$\sigma_{254}=6.7\times10^{-20}$
36	HO2 + hν → OH + O(1D)	3.4×10^{-4}	$\sigma_{254}=2.6\times10^{-19}$
37	H2O2 + OH → HO2 + H2O	1.8×10^{-12}	
38	NO + O3 → NO2 + O2	1.95×10^{-14}	
39	O(1D) + H2 → OH + H	1.2×10^{-10}	

40	OH + H2 → H2O + H	6.67×10^{-15}	
41	NO2 + O(3P) → NO + O2	1.03×10^{-11}	
42	NO2 + O(3P) → NO3	1.61×10^{-12}	
43	H + NO2 → NO + OH	1.28×10^{-10}	
44	NO + NO3 → NO2 + NO2	2.65×10^{-11}	
45	NO2 + O3 → NO3 + O2	3.2×10^{-17}	
46	OH deposition/loss	2.685	
47	RO2 + HO2 → ROOH + O2	2.28×10^{-11}	MCM
48	RO2 + RO2 → 0.38 (Carbonyl + Alcohol + O2)	8.8×10^{-13}	MCM
49	RO2 + RO2 → 0.58 (RO + RO + O2)	8.8×10^{-13}	MCM
50	RO2 + RO2 → 0.04 (LODIMER + O2)	8.8×10^{-13}	Low Oxidized dimer, MCM, Zhao et al. (2018)
51	RO2 + NO2 → RO2NO2	9.0×10^{-12}	p 187 Finlayson - Pitts & Pitts (2000)
52	RO2 → HOMRO2	0.33	3 steps, Jenkin et al (2019); Wang et al. (2017); Ehn et al. (2014)
53	RO → 0.3 (Carbonyl + HO2)	$1.0\times10^{+6}$	MCM, Fraction is empirically determined
54	RO → 0.7 RO2	$1.0\times10^{+6}$	MCM, Fraction is empirically determined
55	HOMRO2 + HO2 → MONOMER	2.28×10^{-11}	MCM
56	HOMRO2 + NO → 0.3 ONs	1.0×10^{-11}	Berndt et al. (2018)
57	HOMRO2 + NO → 0.7 (HOMRO + NO2)	1.0×10^{-11}	Berndt et al. (2018)
58	HOMRO → 0.3 (MONOMER + HO2)	$1.0\times10^{+6}$	MCM, Fraction is empirically determined
59	HOMRO → 0.7 HOMRO2	$1.0\times10^{+6}$	MCM, Fraction is empirically determined
60	HOMRO2 + NO2 → HOMRO2NO2	9.0×10^{-12}	p 187 Finlayson - Pitts & Pitts (2000)
61	RO2NO2 → RO2 + NO2	3.99	Atkinson et al. (1992)
62	HOMRO2NO2 → HOMRO2 + NO2	3.99	Atkinson et al. (1992)
Case 1			
63	HOMRO2 + RO2 → 0.4 (MONOMER + Carbonyl/Alcohol + O2)	8.8×10^{-13}	MCM
64	HOMRO2 + RO2 → 0.6 (HOMRO + RO + O2)	8.8×10^{-13}	MCM
65	HOMRO2 + RO2 → MODIMER + O2	8.0×10^{-11}	Medium Oxidized dimer, Berndt et al. (2018)
66	HOMRO2 + HOMRO2 → 0.4 (MONOMER + MONOMER + O2)	8.8×10^{-13}	MCM
67	HOMRO2 + HOMRO2 → 0.6 (HOMRO + HOMRO + O2)	8.8×10^{-13}	MCM
68	HOMRO2 + HOMRO2 → HODIMER + O2	2.6×10^{-10}	Highly Oxidized dimer, Berndt et al. (2018)
Case 2			
63	HOMRO2 + RO2 → 0.4 (MONOMER + Carbonyl/Alcohol + O2)	1.0×10^{-12}	Zhao et al. (2018)
64	HOMRO2 + RO2 → 0.6 (HOMRO + RO + O2)	1.0×10^{-12}	Zhao et al. (2018)
65	HOMRO2 + RO2 → MODIMER + O2	8.0×10^{-11}	Medium Oxidized dimer, Berndt et al. (2018)
66	HOMRO2 + HOMRO2 → 0.4 (MONOMER + MONOMER + O2)	1.0×10^{-12}	Zhao et al. (2018)
67	HOMRO2 + HOMRO2 → 0.6 (HOMRO + HOMRO + O2)	1.0×10^{-12}	Zhao et al. (2018)
68	HOMRO2 + HOMRO2 → HODIMER + O2	2.6×10^{-10}	Highly Oxidized dimer, Berndt et al. (2018)
Case 3			

63	HOMRO2 + RO2 → 0.4 (MONOMER + Carbonyl/Alcohol + O2)	1.0×10^{-12}	Zhao et al. (2018)
64	HOMRO2 + RO2 → 0.6 (HOMRO + RO + O2)	1.0×10^{-12}	Zhao et al. (2018)
65	HOMRO2 + RO2 → MODIMER + O2	2.0×10^{-12}	Medium Oxidized dimer, Zhao et al. (2018)
66	HOMRO2 + HOMRO2 → 0.4 (MONOMER + MONOMER + O2)	1.0×10^{-12}	Zhao et al. (2018)
67	HOMRO2 + HOMRO2 → 0.6 (HOMRO + HOMRO + O2)	1.0×10^{-12}	Zhao et al. (2018)
68	HOMRO2 + HOMRO2 → HODIMER + O2	2.0×10^{-12}	Highly Oxidized dimer, Zhao et al. (2018)

References (supplemental)

Atkinson, R., Baulch, D. L., Cox, R. A., Hampson, R. F., Kerr, J. A., and Troe, J.: Evaluated Kinetic and Photochemical Data for Atmospheric Chemistry Supplement-Iv - Iupac Subcommittee on Gas Kinetic Data Evaluation for Atmospheric Chemistry, J Phys Chem Ref Data, 21, 1125-1568, Doi 10.1063/1.555918, 1992.

Berndt, T., Scholz, W., Mentler, B., Fischer, L., Herrmann, H., Kulmala, M., and Hansel, A.: Accretion Product Formation from Self- and Cross-Reactions of RO2 Radicals in the Atmosphere, Angewandte Chemie (International ed. in English), 57, 3820-3824, 10.1002/anie.201710989, 2018.

Ehn, M., Thornton, J. A., Kleist, E., Sipila, M., Junninen, H., Pullinen, I., Springer, M., Rubach, F., Tillmann, R., Lee, B., Lopez-Hilfiker, F., Andres, S., Acir, I. H., Rissanen, M., Jokinen, T., Schobesberger, S., Kangasluoma, J., Kontkanen, J., Nieminen, T., Kurten, T., Nielsen, L. B., Jorgensen, S., Kjaergaard, H. G., Canagaratna, M., Maso, M. D., Berndt, T., Petaja, T., Wahner, A., Kerminen, V. M., Kulmala, M., Worsnop, D. R., Wildt, J., and Mentel, T. F.: A large source of low-volatility secondary organic aerosol, Nature, 506, 476-479, 10.1038/nature13032, 2014.

FACSIMILE for Windows 4, v. 4.0.48; MCPA Software Ltd: Faringdon, UK, 2009.

Finlayson-Pitts, B. and Pitts., J.: Chemistry of the Upper and Lower Atmosphere, Academic Press, 1999.

Jenkin, M. E.; Saunders, S. M.; Wagner, V.; Pilling, M. J., Protocol for the development of the Master Chemical Mechanism, MCM v3 (Part B): tropospheric degradation of aromatic volatile organic compounds. Atmos. Chem. Phys., 3, 181-193, 2003.

Jenkin, M. E.; Valorso, R.; Aumont, B.; Rickard, A.R., Estimation of rate coefficients and branching ratios for reactions of organic peroxy radicals for use in automated mechanism construction. Atmos. Chem. Phys., 19, 7671-7717, 2019.

Li, R.; Palm, B. B.; Ortega, A. M.; Hlywiak, J.; Hu, W.; Peng, Z.; Day, D. A.; Knote, C.; Brune, W. H.; de Gouw, J. A.; Jimenez, J. L., Modeling the Radical Chemistry in an Oxidation Flow Reactor: Radical Formation and Recycling, Sensitivities, and the OH Exposure Estimation Equation. The Journal of Physical Chemistry A, 119, (19), 4418-4432, 2015.

Sander, S. P.; Friedl, R. R.; Barker, J. R.; Golden, D. M.; Kurylo, M. J.; Wine, P. H.; Abbat, J. P. D.; Burkholder, J. P.; Kolb, C. E.; Moortgat, G. K.; Huie, R. E.; Orkin, V. L., Chemical Kinetics and Photochemical data for Use in Atmospheric Studies. JPL publication 10-6, 17 (10-6), 2011.

Wang, S., Wu, R., Berndt, T., Ehn, M., and Wang, L.: Formation of Highly Oxidized Radicals and Multifunctional Products from the Atmospheric Oxidation of Alkylbenzenes, Environ Sci Technol, 51, 8442-8449, 10.1021/acs.est.7b02374, 2017.

Watne, A. K., Psichoudaki, M., Ljungstrom, E., Le Breton, M., Hallquist, M., Jerksjo, M., Fallgren, H., Jutterstrom, S., and Hallquist, A. M.: Fresh and Oxidized Emissions from In-Use Transit Buses Running on Diesel, Biodiesel, and CNG, Environmental science & technology, 52, 7720-7728, 10.1021/acs.est.8b01394, 2018.

Zhao, Y., Thornton, J. A., and Pye, H. O. T.: Quantitative constraints on autoxidation and dimer formation from direct probing of monoterpene-derived peroxy radical chemistry, Proc Natl Acad Sci U S A, 115, 12142-12147, 10.1073/pnas.1812147115, 2018.